Desalination and Water Treatment
www.deswater.com

doi:10.5004/dwt.2017.20187

66 (2017) 263–273
March

Using RBF and MLP models in predicting Reactive Red 198 removal from aqueous solution by SBA-15/CTAB composite

Habib-Allah Tayebi

Department of Textile Engineering, Qaemshahr Branch, Islamic Azad University, Qaemshahr, Iran
Tel. +989112160238; email: tayebi_h@yahoo.com

Received 29 April 2016; Accepted 20 August 2016

ABSTRACT

In this study, the mesoporous material SBA-15 were synthesized and then, the surface was modified by the surfactant cetyl trimethyl ammonium bromide (CTAB). Finally, the obtained adsorbent was used in order to remove Reactive Red 198 (RR 198) from aqueous solution. transmission electron microscope (TEM), thermogravimetric analysis (TGA), Fourier transform infra-red spectroscopy (FTIR), X-ray diffraction (XRD), and BET were utilized for the purpose of examining the structural characteristics of the obtained adsorbent. Parameters affecting the removal of RR 198 such as pH, the amount of adsorbent, and contact time were investigated at various temperatures and were also optimized. The obtained optimized condition is as follows: pH = 2, time = 60 min and adsorbent dose = 1 g/l. Moreover, predictive models based on multi-layer perceptron (MLP) and radial basis function (RBF) networks used for predicting the adsorption amount according to the input parameters including pH, dosage, temperature, time and concentration are presented. Two criterions, namely, CC and RMSE between the observed and predicted amounts are used to validate the models. Comparison of the obtained results using these two models showed that the prediction based on the MLP network model is better than the RBF one.

Keywords: SBA-15; CTAB; Reactive Red 198; Adsorption study; Artificial neural network; MLP network; RBF network

1. Introduction

In recent years, the treatment of industrial waste water has gained increasing importance as industrial effluents contain dyes which can result in more pollution of ecosystems [1]. Dyes are used in different industries, especially in textile, leather, pulp, paper, food, plastics, pharmaceutical, cosmetics, and dyestuffs, to name but a few; in particular, textile industries are in the forefront of the use of dyes and the discharge of the largest amount of colored effluent into the environment [2]. Over 70,000 tons of approximately 10,000 different dyes and pigments are used in industries annually worldwide; 20–30% of the dyes are lost in industrial effluents during dyeing and finishing processes due to inefficiencies of the industrial dyeing process [3]. Azo dyes are the largest class of dyes, constituting 60–70% of all dyes produced [4]. Among all forms of dyes, reactive ones are the most difficult to remove due to their high solubility. Azo reactive dyes cause serious ecological problems since they encompass the greatest variety of colors, and at the same time, they may be toxic to some aquatic organisms, animals and humans due to their carcinogenicity which leads to the emergence of mutagenics. Reactive Red 198 is a water soluble azo dye which is widely used for cotton dyeing [5]. A wide range of methods have been developed for the removal of dyes and other colored contaminants from industrial waste water including chemical precipitation, electrolysis, aerobic/ anaerobic biological degradation, chemical coagulation, membrane filtration, flocculation, photochemical degradation and chemical oxidation [6,7]. However, these methods suffer from one or more limitations and are unable to adequately reduce the concentration of dyes to desired levels [8,9]. Adsorption is one method which is widely used because of its high effi-

*Corresponding author.

ciency, ease of operation and low running cost [10]. Various adsorbents such as Fe_3O_4/polyaniline Nano composite [11], activated carbon/polyaniline composite [12], Zeolite [13] have been used for the removal of contaminants from waste water.

In recent years, new hybrid organic–inorganic mesoporous ordered structures are widely being investigated as adsorbents for the removal of heavy metal ions, organic dyes, and other organic compounds [14]. SBA-15 is a new kind of ordered mesoporous molecular sieve exhibiting large and uniform pore size distribution, thick amorphous silica walls, large surface area and remarkable thermal and hydrothermal stability [15–17]. In addition, the surface of SBA-15 can be readily modified by organic groups that can significantly enhance its adsorption capacity and selectivity [18,19].

Modeling and simulation assists us to analyze the effect of various input parameters on the outputs more easily [20]. This results in cost reduction because performing several experiments on all possible amounts of input parameters is normally costly and sometimes very time consuming [21]. AI-based techniques which are widely used for modeling are artificial neural networks (ANN) [21–24], adaptive neuro-fuzzy inference system (ANFIS) [23,24], multiple linear regression (MLR) [21,25], least square-support vector method (LS-SVM) [26], etc. The usage of ANN model for predicting removal of sunset yellow (SY) dye on experimental data is investigated in [27]. Comparison of MLR and ANN models for prediction of methyl orange using tamarisk and AN-NP-AC is performed in [21]. In [23], genetic algorithm optimization is used to optimize the ANN learning for modeling of antibacterial activity of annatto dye on salmonella enteritis. Ghaei et al. has used ANN model to predict the malachite green dye removal by Cu-NWs-AC following conduction of several experiments [25]. ANN based modeling for predicting activated carbons, used for methane storage has been investigated in [28]. Comparison of MLP and RBF networks as tools for flood forecasting is investigated in [29]. In the mentioned studies using ANN based model results, a good agreement between the observed and the predicted data is reported.

In the present work, SBA-15 was functionalized with cetyl trimethyl ammonium bromide (CTAB) and used as an adsorbent for the removal of Reactive Red 198 from aqueous solutions. Besides experimental investigation, MLP and RBF networks are used to predict the adsorption amount based on the input variables including pH, dosage, temperature, time and concentration. The obtained results applying these two models are compared using two criterions.

2. Experimental

2.1. Materials

Materials such as Pluronic P123 surfactant ($EO_{20}PO_{70}EO_{20}$, M_w = 5800), Tetraethylorthosilicate (TEOS, 98%), Hydro chloric acid 37%, sodium hydroxide 99%, and cetyl trimethyl ammonium bromide (CTAB) were supplied from Sigma-Aldrich and Merck. Reactive Red 198 (Reactive Red RB), an anionic dye, was prepared from Dystar (Fig. (1) and Table (1)) and was used as received without further purification. A stock solution of RR 198 (1000 mg/L) was prepared and diluted to the required initial concentration. This dye shows an intense adsorption peak in the visible region at 515 nm. This wave length corresponds to the maximum adsorption peak of RR 198 (λ_{max} = 515).

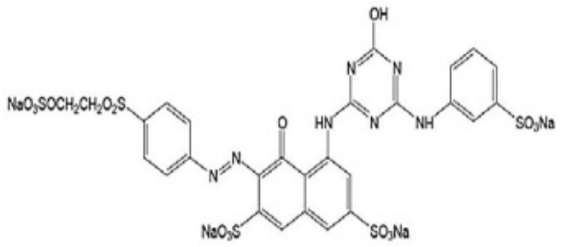

Fig. 1. Small chemical structure of RR 198.

Table 1
Characteristics of RR 198

Name	Reactive Red 198
CAS number	145017-98-7
C.I. number	18221
Formula	$C_{27}H_{18}ClN_7O_{15}S_5{\cdot}_4Na$
Molecular weight	968.21 g/mol
λ_{max}	515 nm

2.2. SBA-15 Synthesis

According to Zhao et al. [30], Mesoporous SBA-15 was synthesized as follows: 12.5 ml of P123 as surfactant and 375 ml of distilled water as well as 75 ml (0.1 N) of HCl were stirred at 42°C. After that, 31.5 ml of TEOS, representing the silica source, was added to the homogeneous mixture. The obtained gel was kept in static conditions at 42°C for 24 h. Next, the temperature was raised to 138°C and maintained for 24 h. After filtration, the obtained powder was transferred to a furnace for calcinations at 550°C for 5 h for the purpose of removing existing organics from its pores.

2.3. SBA-15/CTAB Synthesis

10 ml of distilled water is poured into a beaker and 0.02 g of CTAB as well as 0.1 g of SBA-15 is added to it; then, all these materials are stirred by a mechanical stirrer for 20 min. Finally, the obtained mixture is filtered by filter papers, washed by distilled water and dried in oven at 70°C for 5 h.

2.4. Instrumentation

Transmission electron microscope (TEM) image was provided by Hitachi, HF2000. Field emission scanning electron microscope (FESEM) images were obtained using a TESCAN MIRA3 microscope. Low angle X-ray spectra patterns in the range of 0.6–9 were determined by XPERT-PRO40 kV spectrometer using Cu Kα radiation (λ = 1.5406 Å). Thermogravimetric analysis (TGA) was done with a Shimadzu TGA50H instrument. FT-IR results were

recorded via Shimadzu 4100 FT-IR spectroscopy. The surface area of SBA-15 and the size of holes before and after the Sited CTAB on SBA-15 were measured by Quanta chrome, Chemo BET 3000 TPR/TPD.

2.5. Adsorption studies

Batch experiments were carried out through contacting different amounts of adsorbent (SBA-15/CTAB) with 100 ml dye (RR 198) solution with different initial concentrations (20–400 ppm) at various pH values (2–12) and temperatures of 25, 35 and 45°C. The products were placed in a shaker with 150 rpm velocity for different times (5–120 min). At the end of the process, the adsorbent was separated by centrifuging at 4000 rpm for 30 min. The amount of dye in the solution before and after adsorption process was measured by Jenway 6505 UV-Visible spectrophotometer. The quantity of dye adsorbed on SBA-15/CTAB was estimated using the following Eq. (1):

$$q_e = (C_0 - C_e)\frac{V}{W} \tag{1}$$

where q_e is the quantity of dye adsorbed on SBA-15/CTAB (mg/g), C_0 and C_e are the initial and final dye concentrations (mg/l), respectively. V is the volume of dye bath (l) and W is the weight of adsorbent (SBA-15/CTAB) (g).

2.6. Modelling using MLP and RBF networks

2.6.1. ANN model

ANN models are a valuable forecasting tool in numerous environmental engineering problems. In this research, a comparison between two ANN models namely, MLP and RBF networks, is carried out. The main differences between these two models is that the parameters of the MLP network are nonlinear but those of the RBF networks are linear.

2.6.1.1. MLP network: structure

The MLP model consists of at least three input layer, hidden layer(s) and output layer (Fig. 2a). The MLP model consists of simple processing units called neurons which form the basis for designing the networks [20]. Fig. 2b shows the arithmetic model of a neuron. According to this figure, we can describe a neuron by the following equation:

$$y = \varphi\left(b + \sum_{j=1}^{n} w_j \cdot x_j\right) \tag{2}$$

where $x_1 \ldots x_n$ are input signals; y is the output; $w_1 w_2 \ldots w_{n-1}$ w_n are the synaptic weights of the neuron; b is the bias and $\varphi(.)$ is the activation function. Some basic types of activation functions are sigmoid, piece wise linear, threshold functions. The amount of the error between the model output and the observed response is used to readjust the weight and bias parameters in an iterative fashion with the aim of approaching minimum error.

2.6.1.2. RBF network: structure

RBF network is an alternative to the MLP network, which has linear parameters. Fig. 3 shows schematic diagram of a RBF network. This network is a three-layer feed forward type of network in which the input is transformed by the basis function (typically a Gaussian function which can be defined by a mean and standard deviation) [29]. According to Fig. 3 at the hidden layer, the jth hidden node produces a response H_j as:

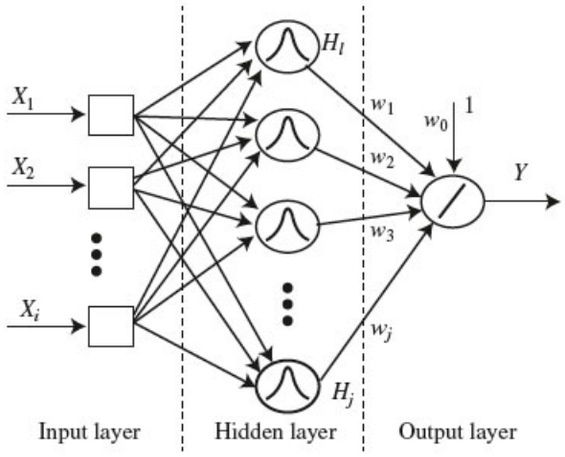

Fig. 3. Structure of the RBF network.

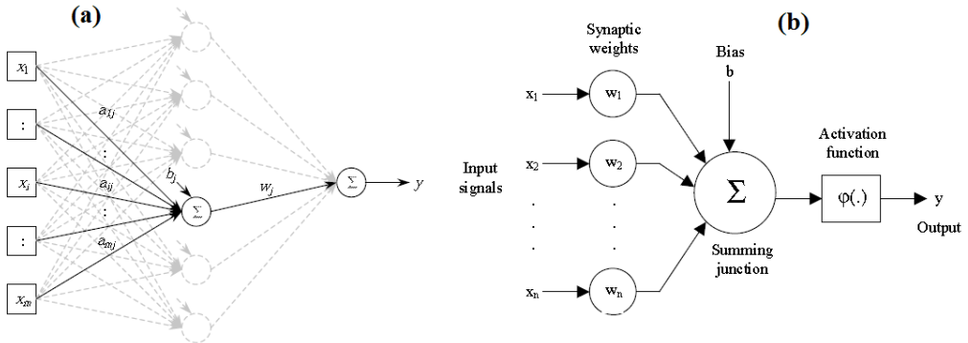

Fig. 2. (a) A feed forward neural network with one hidden layer. (b) Nonlinear model of a neuron.

$$H_j = \exp\left(\frac{-\left\|X - U_j\right\|}{2\sigma_j^2}\right) \quad (3)$$

where $||X - U_j||$ represents the distance between the input X_i and the center of the j th hidden node, U_j.

In this research, the Euclidean norm is used to compute the distance. The final output of the network, at the output layer is obtained by adding the linear combination of the hidden layer node response. The output of the network, Y, can be obtained by the following equation.

$$Y = w_0 + \sum_{j=1}^{m} w_j \cdot H_j \quad (4)$$

The number of hidden nodes can be equal to the number of data in training set (ND), but when ND is large, a few input points can be chosen to represent the entire dataset. The number of nodes can also be reduced by clustering. Each of the RBF centers can be located at the centers of each cluster.

3. Results and discussion

3.1. Characterization analyses

The structure of produced SBA-15 was characterized by transmission electron microscope (TEM) (Fig. 4). The SBA-15 TEM image indicates a hexagonal well-ordered mesoporous structure. The pore diameter of SBA-15 was calculated to be about 6–8 nm which was not much different from the pore size calculated by BJH method. Furthermore, FESEM images of SBA-15 and SBA-15/CTAB are shown in Fig. 5a and 5b, respectively. According to Fig. 5b and Table 2, functionalization with CTAB took place both inside the pores and outside the SBA-15. Low angle X-Ray diffraction patterns of synthesized SBA-15 and SBA-15/CTAB samples are depicted in Fig. 6. These patterns display 3 peaks: one strong peak at 1.035 and two weak peaks at 1.64 and 1.86, respectively, which represent the hexagonal structure of the synthesized silicate mesoporous material. The XRD pattern did not vary after the functionalization of SBA-15 with CTAB.

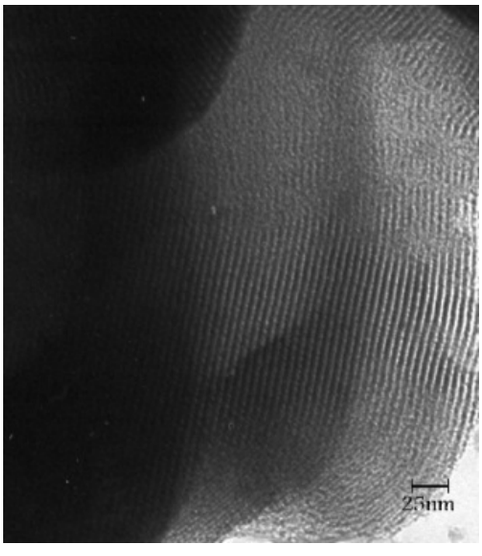

Fig. 4. TEM image of SBA-15 particles.

As it is clear from Fig. 7, no destruction is seen on SBA-15 sample when exposed to temperatures of up to 600°C; this is because of the mineral structure of this compound. However, the sample, the surface of which was modified with CTAB, starts to degrade from 100°C onward and this phenomenon continues until a temperature of 350°C is reached and after that the sample exposed to heat stops degrading; this is because of the thermal destruction of CTAB structure in the SBA-15/CTAB composite. Thus,

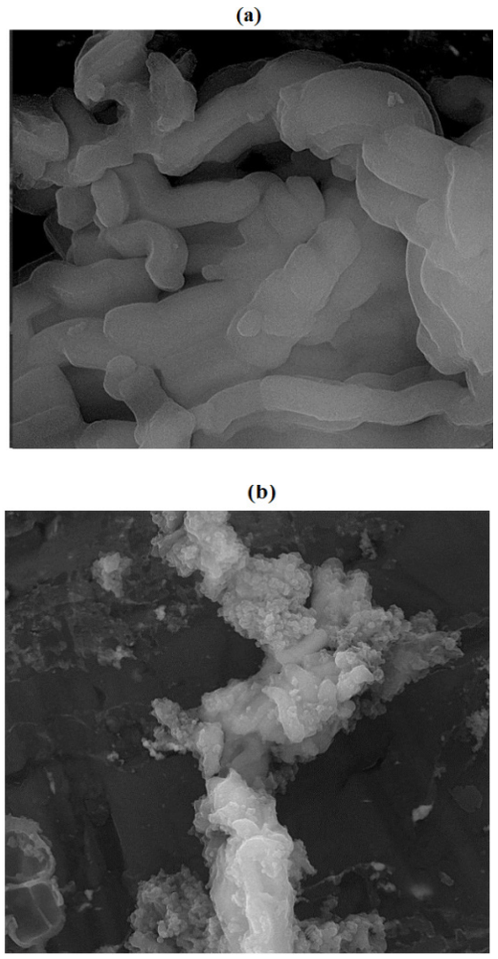

Fig. 5. FESEM images of SBA-15 particles before (a) and after (b) modifying with CTAB.

Table 2
Characteristics of SBA-15 and SBA-15/CTAB samples

Sample	Surface area (BET) (m^2/g)	Pore diameter (BJH) (nm)	Pore volume (BJH) (cm^3/g)
SBA-15	743.5	8.2	0.98
SBA-15/CTAB	246.4	4.6	0.44

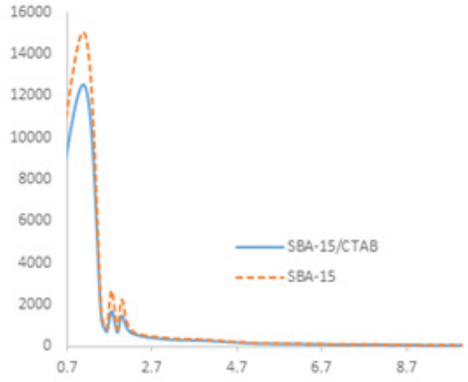

Fig. 6. XRD patterns of SBA-15 and SBA-15/CTAB particles.

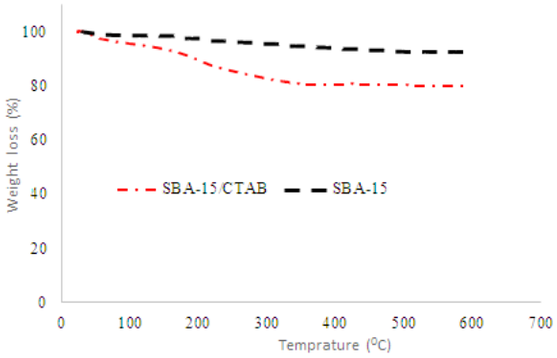

Fig. 7. TGA analysis for SBA-15 and SBA-15/CTAB composite

regarding the obtained data, it can be asserted that the SBA-15/CTAB composite sample is able to stay stable at experiment temperatures which may reach 45°C, at most. The FTIR spectrums of SBA-15 and SBA-15/CTAB samples in the range 400–4000 cm^{-1} are indicated in Fig. 8. Generally, one attribute of Silicate mesoporous materials is the wide and large bands between 3200 and 3500 cm^{-1} which pertains to Silanol groups and water molecules [31]. The wide adsorption band around 1030 to 1240 cm^{-1} is related to the stretching feature of Si–O–Si [31].

The adsorption band in 1076 cm^{-1} represents the asymmetrical stretching of Si–O–Si. The band in 1608 cm^{-1} shows O–H bonds of water molecules. The symmetrical stretching of Si–O–Si occurs in 760 cm^{-1}. The band 894 cm^{-1} is related to Si–OH and represents Silicate mesoporous materials. Some of bands in the FTIR pattern related to SBA-15/CTAB, have either disappeared or their peaks have decreased in the presence of SBA-15; it implies the fact that the CTAB molecular chains have lain on SBA-15 particles. In the case of the SBA-15/CTAB sample, peaks at 2940, and 2826 cm^{-1} ascribed to the long alkyl chain of CTAB further prove the presence of CTAB at the surface of SBA-15 [32].

The N_2 adsorption/desorption isotherms of SBA-15 and SBA15/CTAB are shown in Fig. 9. The SBA-15 sample exhibits a type IV isotherm with a hysteresis loop of type H1 and a sharp increase of adsorbed N_2 at the relative pressure of P/P_0 = 0.62, as expected for mesoporous materials [19,31]. In Table 2, the specific BET surface area, pore volume and average pore diameter of SBA-15 and SBA-15/CTAB are summarized. In the case of SBA-15/CTAB, after functionalization of SBA-15 with CTAB, the inflection point of isotherm shifts to a lower P/P_0; moreover, the decrease in BET surface area, mesopore volume and pore size of SBA-15/CTAB clearly indicates that the CTAB chains have stuck to channels well.

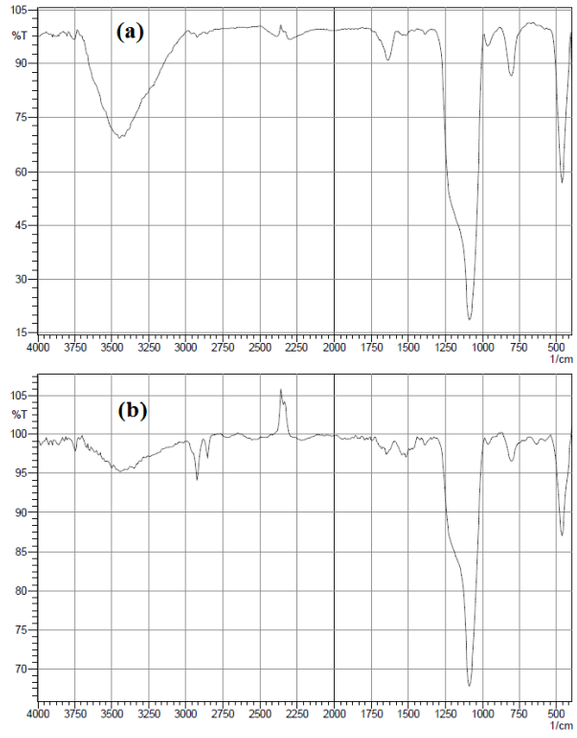

Fig. 8. FTIR spectra of SBA-15 particles before (a) and after (b) modifying with CTAB.

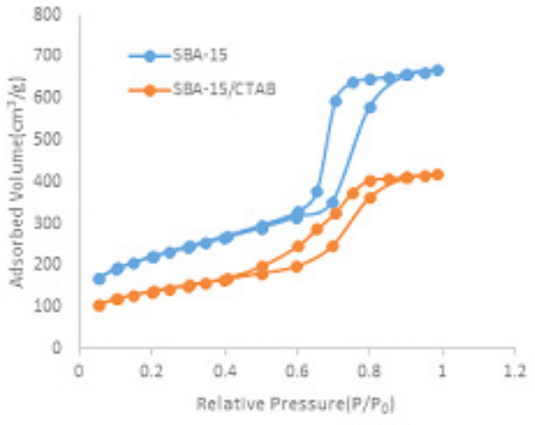

Fig. 9. N_2 adsorption/desorption isotherms of SBA-15 and SBA-15/CTAB.

3.2. Adsorption studies

3.2.1. Effect of pH

In the adsorption process, the pH of solution is one of the most important parameters which controls the adsorption of dye molecules in the adsorption sites. Therefore, a study is carried out in order to optimize pH while other parameters such as the amount of adsorbent (SBA-15/CTAB), dye concentration, and temperature are fixed. Fig. 10 indicates the effect of pH on dye removal efficiency as a function of pH. The primary dye concentration was 20 mg/l and the adsorbent amount equaled 0.1 g. Dye adsorption increases while pH reaches 2 and the maximum adsorption occurs in this case; as in the acidic conditions, more protonation of the adsorbent surface is probable which results in higher dye adsorption.

3.2.2. Effect of adsorbent dosage

The effect of adsorbent amount on dye removal was examined in pH = 2 with 100 ml of the dye solution (20 mg/l) and the result is displayed in Fig. 11. The figure shows that the percentage of dye removal depends on increasing the adsorbent amount and it is raised by the increase of adsorbent to the point that it reaches the highest amount 99% while the adsorbent is 100 mg; this is because when the adsorbent amount rises, the adsorbing sites increase and these sites are more likely to adsorb the dye. However, by increasing the adsorbent amount up to 0.1 g, the adsorption amount was not raised due to the accumulation of adsorbent particles. Therefore, 1 g/l of adsorbent (SBA-15/CTAB) is proven to be the optimum adsorbent amount.

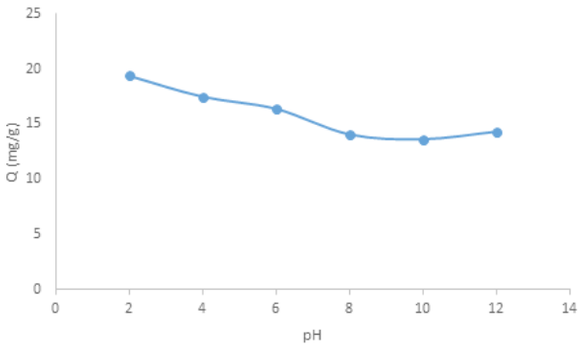

Fig. 10. Effect of pH on RR 198 removal (100 ml of 20 mg/l RR 198, time 2h, T = 25°C and dosage = 100 mg).

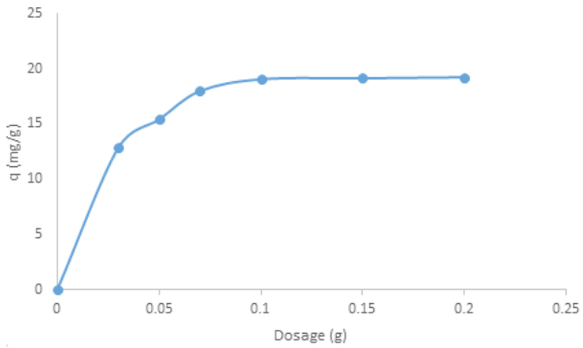

Fig. 11. Effect of dosage on RR 198 removal (100 ml of 20 mg/l RR 198, time 2 h, T = 25°C and pH = 2).

3.2.3. Effect of contact time and temperature

In this section, dye (RR 198) adsorption by the adsorbent (SBA-15/CTAB) was investigated as a function of contact time and the results were displayed in Fig. 12. It is observed that dye adsorption is fast at the beginning and it gradually decreases until it is balanced. At the beginning of the process, changes in adsorption amount happen fast because more adsorbing sites are available; these points gradually decrease and after 60 min, the process reaches balance and the adsorbing sites are saturated. As it is seen in Fig. 12, the adsorption amount was increased by raising the temperature which implies that the adsorption process is endothermic.

3.2.5 Adsorption mechanism

The active surface area of SBA-15 is very large (743.5 m^2/g). Therefore, the contact surface between CTAB and SBA-15 will also be so large and this will lead to the occurrence of many interactions. Considering the neutral pH of the process environment, the amount electro-kinetic charge of SBA-15 is negative (–35 mV) [33]. As it can be seen in Fig. 13, CTAB possesses a positive charge and settles on the Hydroxyl groups of SBA-15 which have negative charges, and by contacting another CTAB molecule, adhered to the dye molecule through its sulfonic group, results in the adsorption of the dye.

3.3. Implementation of ANN models

In this research, we utilize Matlab 2010 Neural Network toolbox to implement the prediction models. For MLP model we applied a 3 layer network with a sigmoid activation function at hidden layer and a linear activation function at output layer and Levenberg Marquardt (LM) back propagation optimization method with 1000

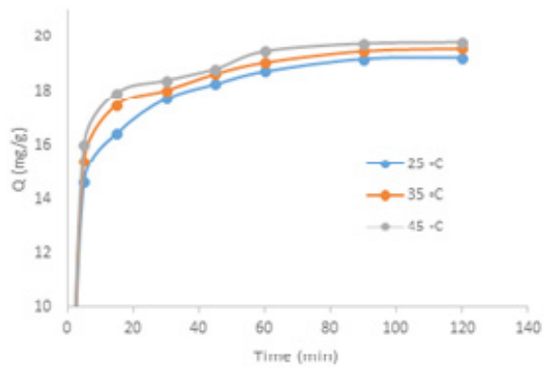

Fig. 12. Effect of time on RR 198 removal (100 ml of 20 mg/l RR 198, dosage= 100 mg, T = 25°C and pH = 2).

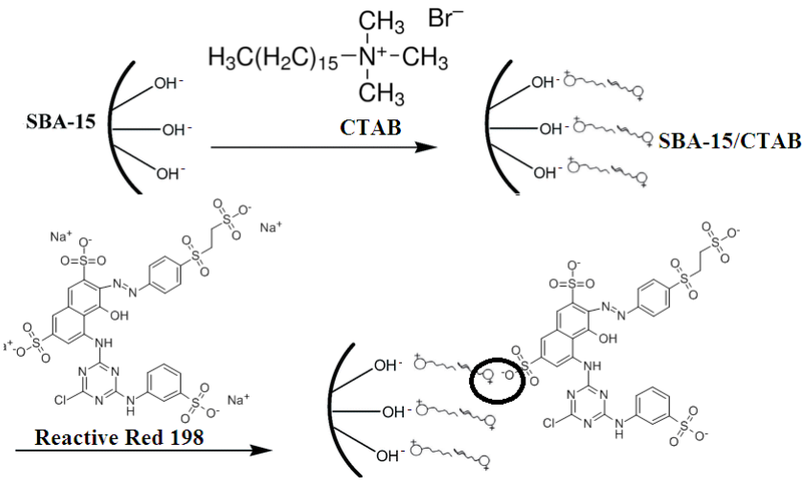

Fig. 13. Schematic illustration of SBA-15 surface modification process with CTAB and dye adsorption mechanism.

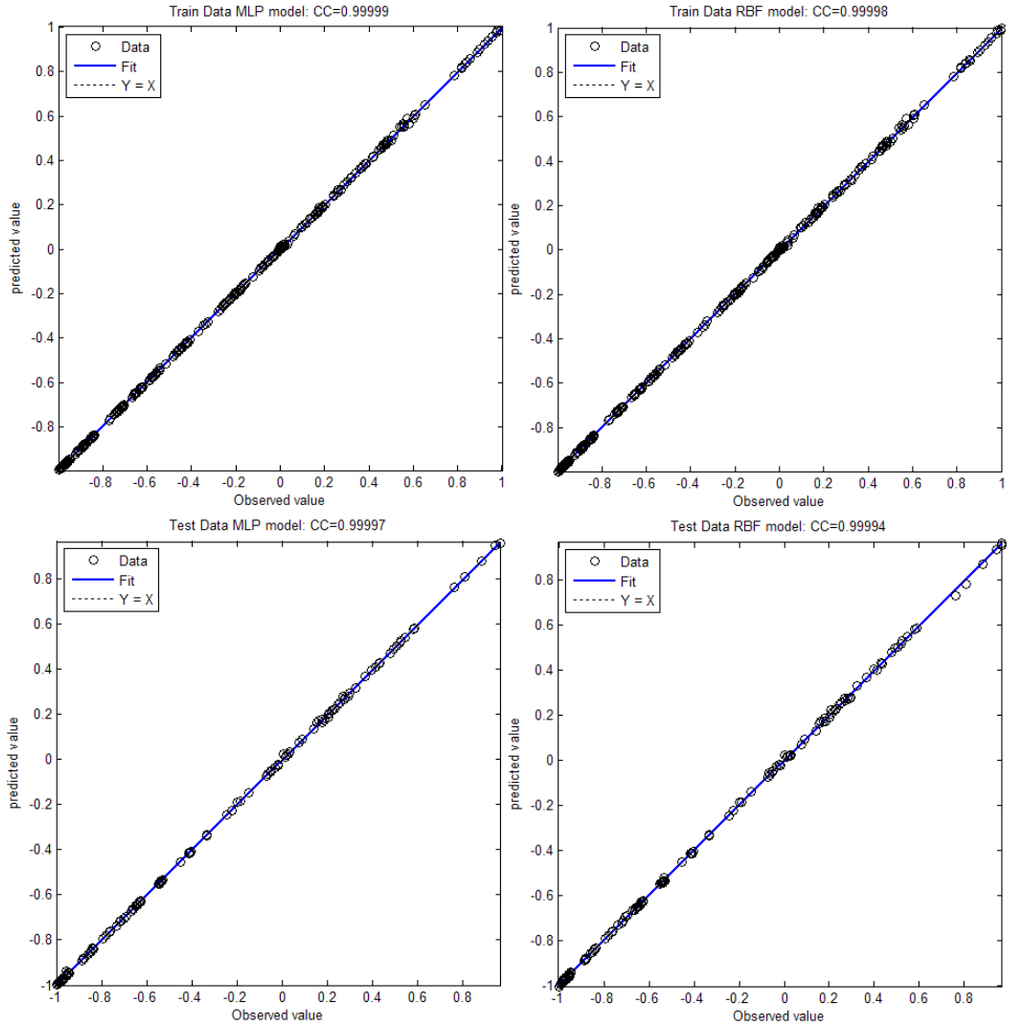

Fig. 14. The correlation plot of observed versus predicted values in training and testing data, applying MLP and RBF networks.

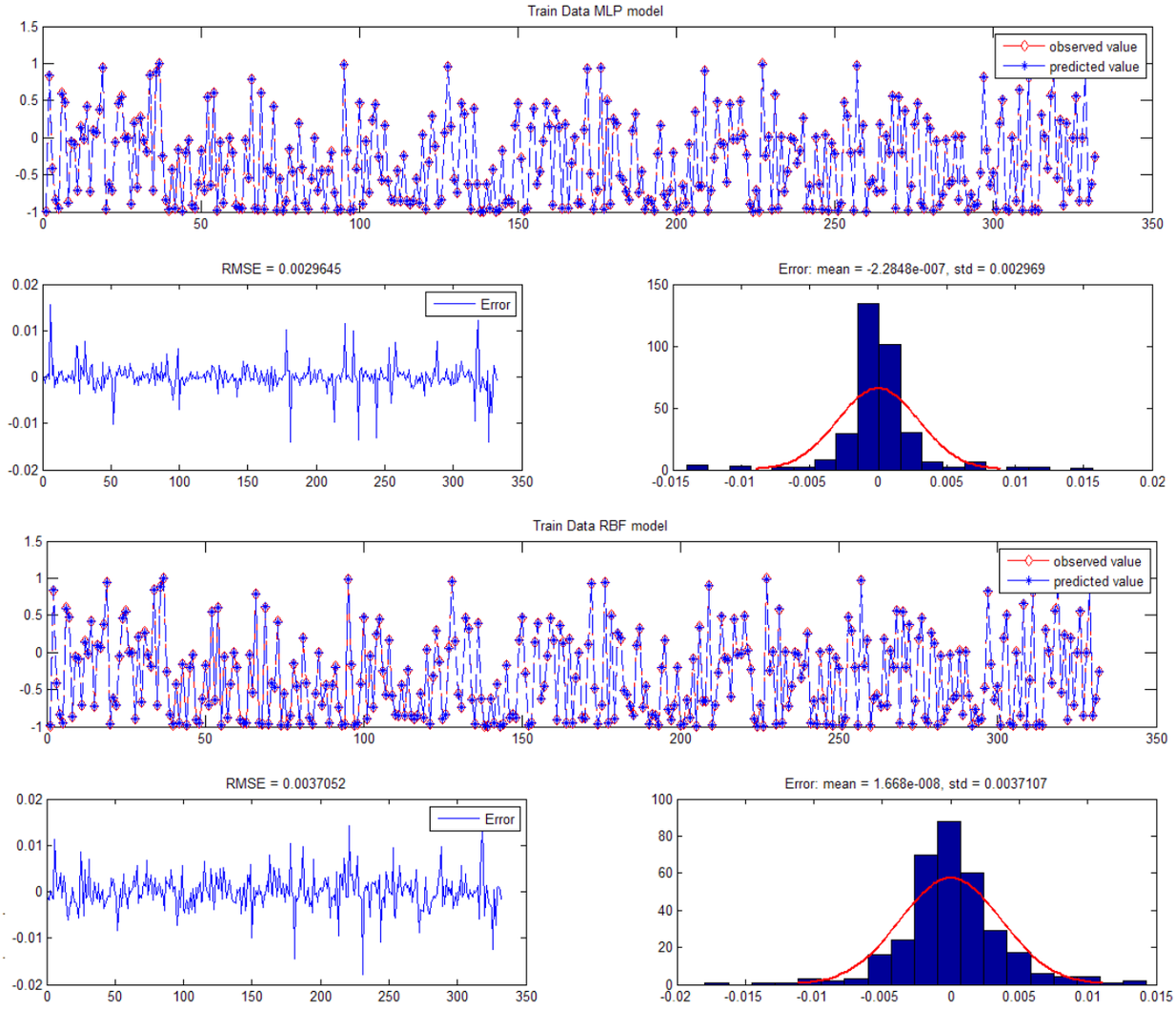

Fig. 15. Evaluating the prediction model in training data using MLP and RBF models. The distribution of observed and predicted values, the Error amounts between the observed and the predicted values and the histograms of errors in training data, using the two models are plotted in this image.

iterations. For RBF model we used newrb() function of the neural network toolbox of Matlab 2010. The training and testing processes are carried out according to the observed data by performing some experiments. Each data record consists of an output (adsorption rate) and five input parameters (pH, dosage, temperature, time and concentration). 70% of data was used as training data and the remaining 30% is considered as testing data. The training records are selected randomly from the whole data.

Two criterions, namely, CC (correlation coefficient) and RMSE (root mean square error) are used for evaluating the models. CC stands for the correlation between the amounts of observed and the obtained output predicted by the models.

In training and testing data, CC can be calculated through the following equation:

$$CC = \frac{\sum_i (y_i - \bar{y})(o_i - \bar{o})}{\sqrt{\sum_i (y_i - \bar{y})^2 \sum_i (o_i - \bar{o})^2}} \quad (5)$$

where y_i and o_i are the observed and the predicted values, respectively. The variation patterns of observed and predicted data in batch process in training and testing data are presented in Fig. 14.The values of CC are shown above every image in Fig. 14.

Another criterion which is used for evaluating the model is RMSE that is calculated through the following equation in testing and training data.

$$RMSE = \sqrt{\frac{\sum_i (y_i - o_i)^2}{N}} \quad (6)$$

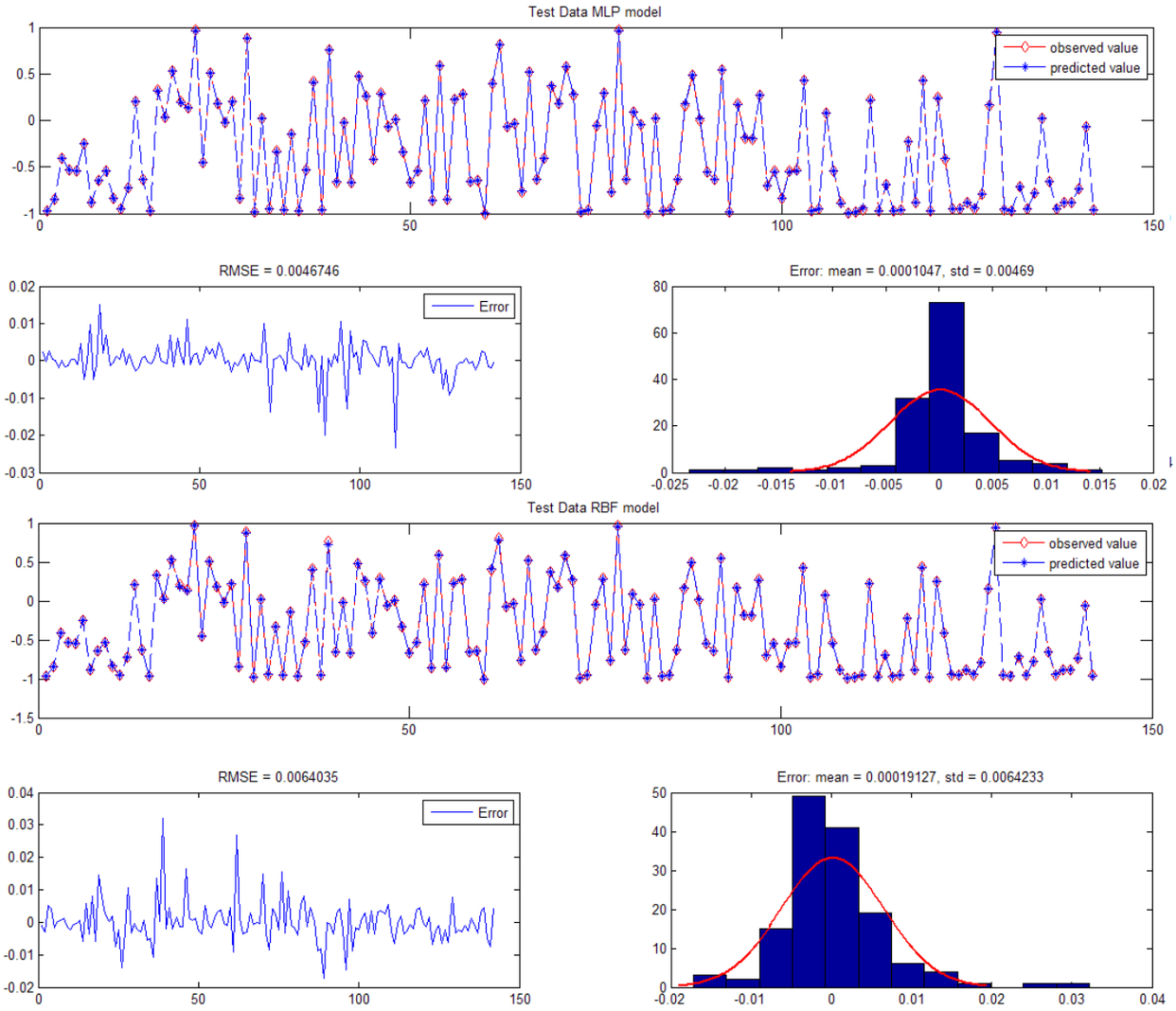

Fig. 16. Evaluating the prediction model in testing data using MLP and RBF models. The distribution of observed and predicted values, the Error amounts between the observed and the predicted values and the histograms of errors in testing data, using the two models are plotted in this image.

where N is the number of data points. The observed and the predicted values for testing and training data and the amount of RMSE value in each set are shown in Figs. 15 and 16. The images in Figs. 15 and 16 and the obtained parameters imply the accuracy of the trained model in predicting the adsorption amount based on its inputs.

Diagrams in Fig. 17 represent the dependence among the number of nodes at hidden layer of MLP network and the obtained RMSE amount in testing and training data. It can be concluded that the MLP network containing 15–18 nodes at hidden layer can be chosen as the best model for prediction. Also the diagrams of RMSE amount of the RBF model considering various amounts of spread and maxneuron parameters are plotted in Fig. 17.

As it was mentioned, training and testing data are selected from the whole data randomly (training data are randomly chosen first and then, the rest of the data are devoted to testing). Every random selection results in networks with minor differences in the parameters and different evaluative criterions. The results of systems displayed in Figs. 15 and 16 are related to one experiment. In order to investigate the accuracy of the proposed models more realistically, we performed training and testing 50 times and RMSE parameter is obtained per experiment (in each run the training and testing data are chosen randomly). Table 3 depicts the average and standard deviation of RMSE in testing and training data obtained after performing all the experiments. It has to be mentioned that in these experiments, according to Fig. 17a–c, the max-neuron and spread parameters of newrb() function are set to 100 and 2.5, respectively. The number of nodes at hidden layer in MLP model is set to 15.

The obtained results confirm the strength of these models in predicting the outcomes and according to Fig. 17d and

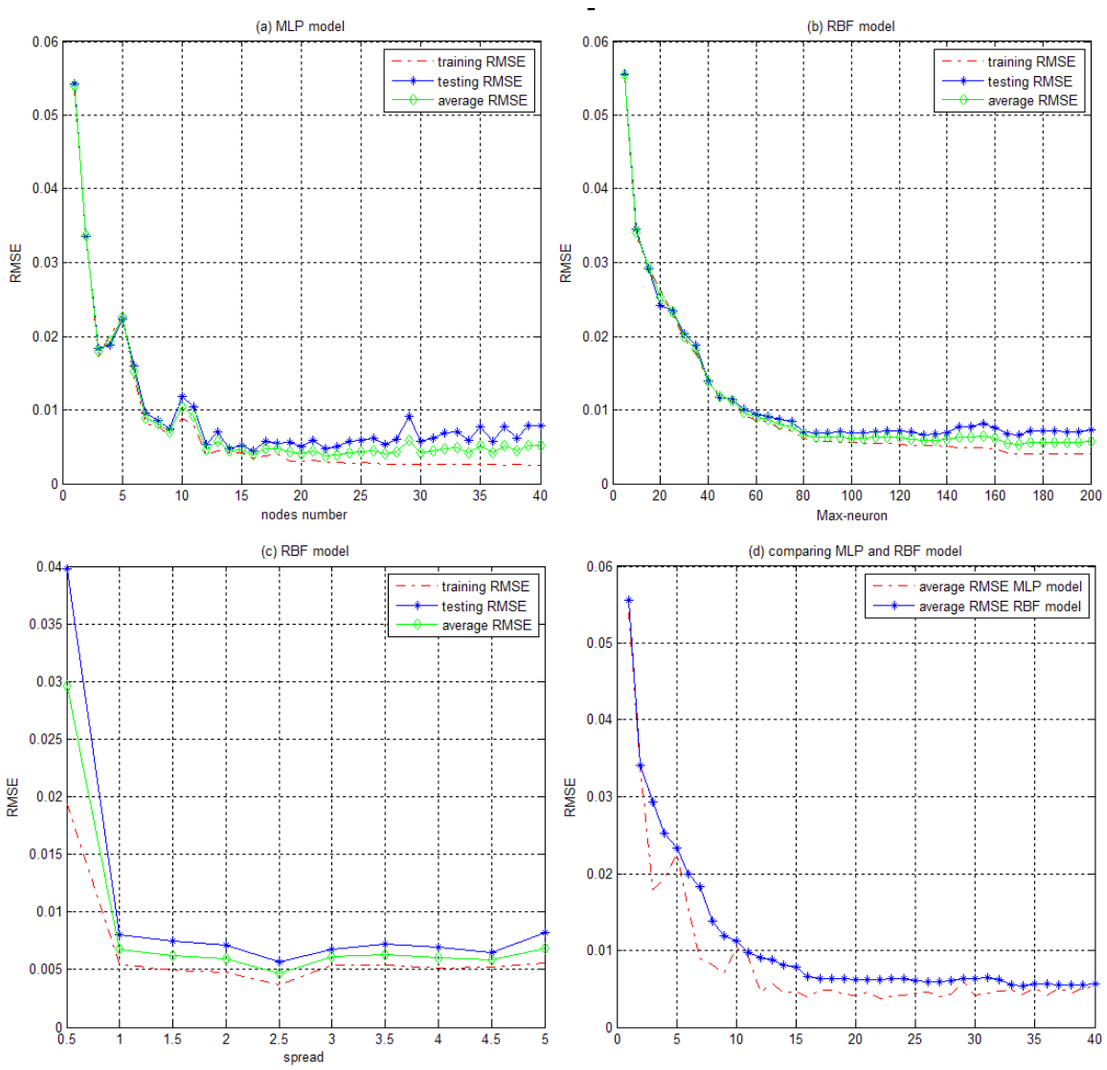

Fig. 17. (a) The RMSE amounts versus the number of hidden neurons in MLP model; (b), (c) The RMSE amounts versus the maximum number of neurons and spread amount, respectively. (d) The average RMSE of training and testing data for MLP and RBF networks.

Table 3
Performance evaluation of the two models in various experiments. Mean and standard deviation of the RMSE parameters obtained after 50 runs in training and testing data.

RMSE	Training data		Testing data	
	Mean	Std	Mean	Std
MLP network	0.0035	0.0004	0.0067	0.0018
RBF network	0.0042	0.0005	0.0074	0.0012

Table 3, it can be concluded that the prediction based on the MLP network model is better than the RBF network.

4. Conclusions

In this work, SBA-15 was synthesized and modified with CTAB. According to the obtained results, SBA-15/CTAB adsorbent had high efficiency for RR 198 removal from aqueous media. Optimal conditions of RR 198 removal was obtained at pH = 2, contact time of 60 min and dosage of 1 g/l. MLP and RBF Networks have been applied to predict the adsorption rate based on the input variables including temperature, pH, time, dosage, concentration. To validate the models, the predicted values are compared to the measured ones. Two criterions, namely, CC and RMSE are used for comparison. According to the obtained results, a 3-layer MLP network with 15 neurons in the hidden layer and a RBF model with approximately 100 nodes and the spread amount of 2.5 are used for prediction. The high amount of CC (approximately 0.9998 ± 0.0001 for MLP and 0.9996 ± 0.0009 for RBF model) and the low amount of RMSEs (approximately 0.0051 ± 0.0011 for MLP and 0.0058 ± 0.0009 for RBF model) in testing and training data represent the high efficiency of the predictive models. Finally, the results indicate that MLP model is more suitable than the RBF model in predicting and simulating the adsorption rate.

References

[1] M. Anbia, S. Asl Hariri, S.N. Ashra_zadeh, Adsorptive removal of anionic dyes by modified nanoporous silica SBA-3, Appl. Surf. Sci., 256 (2010) 3228–3233.

[2] F. Esther, T. Cserhati, G. Oros, Removal of synthetic dyes from wastewaters: a review, Environ. Int., 30 (2004) 953–971.

[3] I.A.W. Tan, A.L. Ahmad, B.H. Hameed, Adsorption of basic dye on high-surface-area activated carbon prepared from coconut husk: Equilibrium, kinetic and thermodynamic studies, J. Hazard. Mater., 154 (2008) 337–346.

[4] C. Máximo, M. Amorim, M. Costa-Ferreira, Biotransformation of industrial reactive azo dyes by Geotrichum sp. CCMI 1019, Enzyme Microb. Technol., 32 (2003) 145–151.

[5] B. Manu, S. Chaudhari, Decolorization of indigo and azo dyes in semicontinuous reactors with long hydraulic retention time, Process Biochem., 38 (2003) 1213–1221.

[6] A. Maleki, A.H. Mahvi, R. Ebrahimi, Y. Zandsalimi, Study of photochemical and sonochemical processes efficiency for degradation of dyes in aqueous solution. Korean J. Chem. Eng., 27 (2010) 1805–1810.

[7] M. Shirmardi, A. Mesdaghinia, A.H. Mahvi, S. Nasseri, R. Nabizadeh, Kinetics and equilibrium studies on adsorption of acid red 18 (Azo-Dye) using multiwall carbon nanotubes (MWCNTs) from aqueous solution. E-J. Chem., 9 (2012) 2371–2383.

[8] N. Dizge, C. Aydiner, E. Demirbas, M. Kobya, Adsorption of reactive dyes from aqueous solutions by ash: kinetic and equilibrium studies, J. Hazard. Mater., 150 (2008) 737–746.

[9] P. Caizares, F. Martínez, C. Jiménez, Coagulation and electrocoagulation of wastes polluted with dyes, Environ. Sci. Technol., 40 (2006) 6418–6424.

[10] V.K. Gupta, A. Mittal, L. Krishnan, V. Gajbe, Adsorption kinetics and column operations for the removal and recovery of malachite green from wastewater using bottom ash, Sep. Purif. Technol., 40 (2004) 87–96.

[11] H.A. Tayebi, Z. Dalirandeh, A. Shokuhi Rad, A. Mirabi, E. Binaeian, Synthesis of polyaniline/Fe_3O_4 magnetic nanoparticles for removal of reactive Red 198 from textile waste water: kinetic, isotherm, and thermodynamic studies, Desalin. Water. Treat., (2016), doi: 10.1080/19443994.2015.1133323.

[12] D. Zareyee, H.A. Tayebi, H. Javadi, Preparation of polyaniline/activated carbon composite for removal of reactive Red 198 from aqueous solution, Iranian J. Org. Chem., 4 (2012) 799–802.

[13] H. Javadian, F. Ghorbani, H.A. Tayebi, S.M. Hosseini Asl, Study of the adsorption of Cd (II) from aqueous solution using zeolite-based geopolymer, synthesized from coal y ash; kinetic, isotherm and thermodynamic studies, Arabian J. Chem., 8 (2015) 837–849.

[14] M. Mureseanu, A. Reiss, I. Stefanescu, E. David, Modified SBA-15 mesoporous silica for heavy metal ions remediation, Chemosphere, 73 (2008) 1499–1504.

[15] A. Katiyar, S. Yadav, P.G. Smirniotis, N.G. Pinto, Synthesis of ordered large pore SBA-15 spherical particles for adsorption of biomolecules, J. Chromatogr., 1122 (2006) 13–20.

[16] K.De. Witte, P. Cool, I.De. Witte, L. Ruys, Multistep Loading of Titania Nanoparticles in the Mesopores of SBA-15 for enhanced photocatalytic activity, J. Nanosci. Nanotechnol., 7 (2007) 2511–2515.

[17] S.E. Rankin, B. Tan, H.J. Lehmler, K.P. Hindman, Well-ordered mesoporous silica prepared by cationic uorinated surfactant templating, Microporous Mesoporous Mater., 73 (2004) 197–202.

[18] J.H. Yim, D.I. Kim, J.A. Bae, Y.K. Park, Removal of formaldehyde over amine functionalized SBA-15, J. Nanosci. Nanotechnol., 11 (2011) 1714–1717.

[19] M. Shafiabadi, A. Dashti, H.A. Tayebi, Removal of Hg (II) from aqueous solution using polypyrrole/SBA-15 nanocomposite: Experimental and modeling, Synth. Met., 212 (2016) 154–160.

[20] K. Yetilmezsoy, B. Ozkaya, M. Cakmakci, Artificial intelligence-based prediction models for environmental engineering, Neural Netw. World, 21 (2011) 193.

[21] M. Ghaedi, A.M. Ghaedi, A. Ansari, F. Mohammadi, A. Vafaei, Artificial neural network and particle swarm optimization for removal of methyl orange by gold nanoparticles loaded on activated carbon and Tamarisk, Spectrochim. Acta, Part A., 132 (2014) 639–654.

[22] H. Gharibi, A.H. Mahvi, R. Nabizadeh, H. Arabalibeik, M. Yunesian, M.H. Sowlat, A novel approach in water quality assessment based on fuzzy logic. J. Environ. Manage., 112 (2012) 87–95.

[23] M. Yolmeh, M. Habibi Najafi, F. Salehi, Genetic algorithm-artificial neural network and adaptive neuro-fuzzy inference system modeling of antibacterial activity of annatto dye on Salmonella enteritidis, Microb. Pathogenesis, 67 (2014) 36–40.

[24] B. Rahmanian, M. Pakizeh, S.A.A. Mansoori, M. Esfandyari, D. Jafari, H. Maddah, A. Maskooki, Prediction of MEUF process performance using artificial neural networks and ANFIS approaches, J. Taiwan Inst. Chem. Eng., 43(2012) 558–565.

[25] M. Ghaedi, E. Shojaeipour, A.M. Ghaedi, R. Sahraei, Isotherm and kinetics study of malachite green adsorption onto copper nanowires loaded on activated carbon: artificial neural network modeling and genetic algorithm optimization, Spectrochim. Acta, Part A., 142 (2015) 135–149.

[26] M. Ghaedi, A.M. Ghaedi, M. Hossainpour, A. Ansari, M.H. Habibi, A.R. Asghari, Least square-support vector (LS-SVM) method for modeling of methylene blue dye adsorption using copper oxide loaded on activated carbon: Kinetic and isotherm study. J. Ind. Eng. Chem., 20(2014) 1641–1649.

[27] A.M. Ghaedi, M. Ghaedi, P. Karami, Comparison of ultrasonic with stirrer performance for removal of sunset yellow (SY) by activated carbon prepared from wood of orange tree: Artificial neural network modeling, Spectrochim. Acta, Part A., 138 (2015) 789–799.

[28] S. Rashidi, A. Ahmadpour, N. Jahanshahi, M.J. Darabi Mahboub, H. Rashidi, Application of artificial intelligent modeling for predicting activated carbons properties used for methane storage, Sep. Sci. Technol., 50 (2015) 110–120.

[29] A.W. Jayawardena, D.A.K. Fernando, M.C. Zhou, Comparison of multilayer perceptron and radial basis function networks as tools for flood forecasting, IAHS Publications-Series of Proceedings and Reports-Intern Assoc Hydrological Sciences, 239 (1997) 173–182.

[30] D. Zhao, Q. Huo, J. Feng, B.F. Chmelka, Nonionic triblock and star diblock copolymer and oligomeric surfactant syntheses of highly ordered, hydrothermally stable, mesoporous silica structures, J. Am. Chem. Soc., 120 (1998) 6024–6036.

[31] Q. Cheng, V. Pavlinek, A. Lengalova, C. Li, Y. He, Conducting polypyrrole confined in ordered mesoporous silica SBA-15 channels: preparation and its electrorheology, Micropor. Mesopor. Mater., 93(1) (2006) 263–269.

[32] A. Barhoum, H. Rahier, R.E. Abou-Zaied, Effect of cationic and anionic surfactants on the application of calcium carbonate nanoparticles in paper coating, ACS Appl. Mater. Interfaces., 6 (2014) 2734–2744.

[33] J.M. Rosenholm, M. Lindén, Towards establishing structure–activity relationships for mesoporous silica in drug delivery applications, J. Control. Release., 128(2) (2008) 157–164.